Reconstruction in Air of an Iron Passive Film Formed at −0.4 V in a Borate Buffer Solution

Huihua Deng, Ikuo Ishikawa, Michio Yoneya, and Hiroshi Nanjo*

AIST Tohoku, National Institute of Advanced Industrial Science and Technology, Nigatake 4-2-1, Sendai 983-8551, Japan

Received: December 1, 2003; In Final Form: March 28, 2004

The reconstruction in air of passive films on iron formed at −0.4 V in a borate buffer solution was investigated by STM and galvanostatic cathodic reduction. With exposure to air (<30% RH), the apparent thickness rapidly increased in initial stages until a critical exposure duration of about 130 min, and after a transition between 130 and 360 min, slowly increased in the following stages, and the changes of surface structures from the amorphous state to short-range order and then to long-range order and further to crystal structures with a wide terrace were observed. These processes are suggested to be attributed to rapid dehydration of Fe^{3+} and Fe^{2+} hydroxides and partial rapid oxidation upon removal from electrolytic solution after passivation, steady oxidation in air until the attainment of a passive state to be more protective one at $t = t_c$, and reconstruction in air, respectively. The reconstruction process remarkably improved the resistance of the passive films against open-circuit breakdown. The behavior of passive films formed at −0.4 V observed during air exposure is actually self-protective.

Introduction

The nature of passive films grown on iron in a borate buffer solution has been studied by in situ and ex situ analytical methods for several decades. The stability in air of passive films formed at different potentials in the passive region is an important factor in keeping the identical result for both in situ and ex situ experiments because specimens transferring for ex situ analysis were exposed to air in most cases. In fact, passive films on Fe formed at low potentials are unstable in air, while those formed at higher potentials are resistant to air oxidation though a fraction of a monolayer on the outermost surface uptakes oxygen from air.[1−4]

Concerning the structure and composition of passive films formed at higher potentials by the potential-step method, most ex situ and in situ experimental results are identical though there are some doubts about the γ-Fe_2O_3 (outer)/Fe_3O_4 (inner) bilayer structure. The first in situ investigation on the composition of passive films was done by in situ Mössbauer spectroscopy.[4−6] The in situ passive film did not resemble any of the stoichiometric crystalline oxy-hydroxide, hydroxides, and oxides including γ-Fe_2O_3, Fe_3O_4, and $Fe_2O_3 \cdot H_2O$ but appeared to be more like amorphous iron oxide(III) with highly distorted bonding, iron containing polymer, and bionuclear iron compounds containing dioxy and dihydroxy bridging bonds between the iron atoms, where iron is in an octahedral high-spin state.[5] It was also investigated by the subsequent surface-enhanced Raman spectroscopy (SERS)[7−10] that passive films formed over a wide range of potentials resemble Fe_3O_4 in addition to the hydroxide-like species. It was suggested in most recent experiments that the passive film is either amorphous or a spinel structure (similar to γ-Fe_2O_3 and Fe_3O_4) identified by in situ X-ray absorption near-edge structure (XANES) data with high resolution.[11,12]

The passive film formed in the early stages of passivation was not any of the well-defined crystalline oxides because the oxide film is formed by a rapid nucleation and growth under the strong applied electric filed ($\sim 10^6$ V cm^{-1}) at high passivation potential. After passivation for longer time and/or exposure to air, the passive films formed at higher potentials show more crystallinity.[13−18] The crystalline nature of passive films formed at higher potential was disclosed early by ex situ electron diffraction.[13] The passive films, formed on Fe(112) at −0.19 V/SCE and on polycrystalline iron at 0.85 V/SCE in a borate buffer solution, show a cubic structure with an average lattice parameter of 8.37 and 8.40 Å, respectively. This means that the passive film has the spinel structure, which was further supported by electron diffraction studies performed by other workers.[14,15] It was shown by in situ synchrotron X-ray diffraction (XRD) that the film structure is based on Fe_3O_4 structure with many cationic vacancies.[16,17] Recently the surface nature of the passive film grown on iron in a borate buffer solution has been studied by scanning tunneling microscopy (STM) and atomic force microscopy (AFM).[16−23] Ex situ and in situ STM examinations[18] directly demonstrated the crystallinity of passive films formed at +0.4 V/MSE (+0.8 V/SCE) in that the triangular lattice observed is consistent with that of oxygen ions on the (111) face of the spinel structure.

An air-formed oxide film was estimated by earlier electron diffraction[24] to be composed of a nanocrystal of <3 nm lateral dimension. The ex situ Mössbauer results similar to the in situ data recorded in refs 4−6 were alternatively interpreted in terms of a γ-Fe_2O_3-like film with a very fine particle size.[25] The broadening of the SERS peaks was attributed to an amorphous structure or very fine grain size.[26] On the basis of the peak broadening in the in situ synchrotron XRD data,[16,17] it was concluded that the film formed at +0.4 V/MSE (+0.8 V/SCE) is nanocrystalline with a grain size of 5−8 nm in-plane and about 3 nm out-of-plane. It was confirmed by ex situ and in situ STM[19] that the average lateral size of the passive film in

* To whom correspondence should be addressed. Phone: +81-22-237-5211. Fax: +81-22-239-0629. E-mail: hi-nanjo@aist.go.jp.

10.1021/jp0376673 CCC: $27.50
Published on Web 06/03/2004

borate buffer solution was observed to be about 5 nm. Therefore it is accepted that the structure of passive films formed at higher anodic potentials is related to γ-Fe_2O_3 or Fe_3O_4 structure with nanocrystallinity in which the outermost layer is the γ-Fe_2O_3-like structure.

The instability in air of Fe passive films formed at low potentials led to significant variation in results between in situ and ex situ analysis and even produced spurious effects during experimental measurements. For Fe passive films formed at low potentials, the time dependences of chemical composition and film thickness were first examined by the labeling analysis of ^{18}O SIMS[1,2] upon air exposure after removal from solution, and significant local structural changes upon drying or dehydration in air were monitored by Mössbauer analysis.[3−5] However, there is little information on reconstruction in air of surface crystal structure of the passive film on iron formed at low potentials.

The surface reconstruction in air was demonstrated by ex situ STM for passive films formed on alloys[27,28] after passivation in 0.1 M H_2SO_4. The surface structures on Fe−Cr alloys depend on Cr contents after passivation for 5 min.[27] The surfaces on Fe−15Cr alloy show more crystallinity. The extent of crystallinity of passive films formed on Fe−Cr alloy with 18 and 21 atom % of Cr[27] and on 304 stainless steel (SS304)[28] depends on the exposure time in air. The films formed on alloy with 25 atom % of Cr are normally disorder within exposure to air for 72 h,[27] which shows independence of exposure time in air. Moreover, it seems that in situ STM observation[29,30] emphasizes the effect of passivation time, especially for alloys with higher Cr content. After passivation for 1 h, long-range order was observed by in situ STM on Fe−13.8Cr and the short-range order on Fe−Cr alloy with 14.7 and 16.5 atom % of Cr.[29] The disorder with circular atomic protrusions observed on Fe−22Cr (110) by in situ STM becomes the long-range order with increasing passivation time from 2 to 63 h in diluted sulfuric acid.[30] Thus, there are some arguments that the long-range order gradually arises from a grain growth or crystallization process during the passivation or reconstruction during air exposure because the possible chemical or structural change of the passive film occurred during air exposure upon removal from electrolyte.[1,2] In addition, the effect of air exposure on surface structures was not reported in detail. In this paper, the reconstruction in air of iron passive films formed at −0.4 V/SCE in a borate buffer solution will be investigated by STM in combination with galvanostatic cathodic reduction and the measurement of open-circuit potential in the borate buffer solution.

Experimental Section

Specimens for galvanostatic cathodic reduction and measurement of open-circuit potential (E_{OC}) decay are polycrystalline iron disks (99.99%) 10 mm in diameter and 2 mm thick. Before electrochemical treatments and measurements, they were polished with successive grades of emery paper and further polished with 9 and 3 μm diamond suspensions and 0.05 μm colloidal alumina suspensions (Buehler), which gave a mirrorlike surface. Specimens for STM imaging are thin films of polycrystalline pure iron prepared by the argon plasma sputter-deposition technique at room temperature (RT). The as-sputtered specimens finally obtained are 570-nm multilayer structures with Fe(II)/platinum (Pt)/Fe(I) on a polished silicon wafer 76 mm in diameter, in which the Fe layer (I) has a role of improving the binding between Pt and SiO_2 and the Pt layer is deposited to prevent Si in the wafer from diffusing into the working Fe layer (II). The purity of the target is 99.99% Fe. A typical specimen is a 5 × 5 mm^2 rectangular plate.

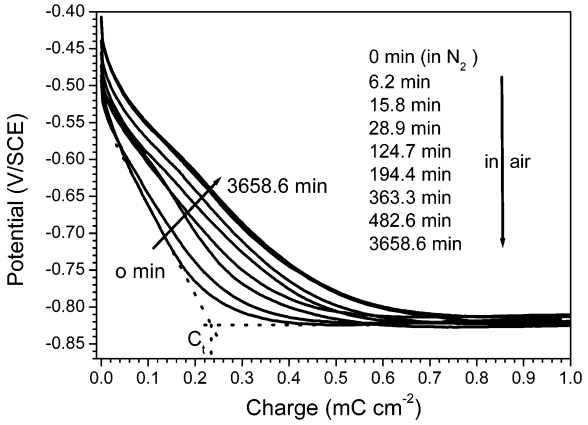

Figure 1. Potential decay curves in galvanostatic cathodic reduction for passive films exposed to air for different duration after passivation at −0.4 V/SCE for 30 min in a borate buffer solution. The dotted line indicates the determination of the total reduction charge with <5% deviation. The arrow indicates the evolution of the first potential arrest with increasing exposure time in air.

The cell with a specimen electrode, a saturated calomel reference electrode (SCE), and a platinum counter electrode was electrochemically controlled by a potentiostat and function generator from Hokuto-Denko Corporation. The electrolyte was the pH 8.4, 0.136 M borate buffer solution (7.07 g L^{-1} H_3BO_3 + 8.17 g L^{-1} $Na_2B_4O_7{\cdot}10H_2O$) made from analytical grade chemicals and distilled water. All the electrochemical experiments were carried out in solutions deaerated by a nitrogen gas and thermostated at the desired temperature. Specimens were cathodically reduced at −1.1 V for 25 min and −1.5 V for 5 min to remove the native oxide on the specimen surface, and then were passivated by stepping the potential to −0.4 V for 30 min and removed from the solution, rinsed with distilled water, dried with cool air, and exposed to air. After exposure to air at RT for the desired duration, subsequent galvanostatic cathodic reduction at a constant current density of −2 μA cm^{-2} and measurement of E_{OC} decay were done in the remaining identical solution deaerated by a nitrogen gas and thermostated at 25.0 ± 0.5 °C. An experimental error with ±0.01 V for the potential decay measurements happened because there was a minor amount of Fe^{2+} ions (10^{-8} M) generated during the cathodic pretreatment of air-formed oxide films on the specimen's surface. The relative humidity (RH) in air exposure was less than 30% and the time was counted from removal of the specimens from solution until the electrochemical measurements or STM observation.

After passivation treatment at −0.4 V, evolution of surface structures with exposure time in air was imaged by a Nanoscope IIIa STM (Digital Instruments). The bias and tunneling current were 0.3−1.5 V and 0.6−2 nA, respectively. Tunneling probe tips were made from tungsten wire anodically etched in 1 M KOH solutions. The STM images presented here were recorded in the constant-current mode and have been processed by high frequency cutoff filters. Atomic spacing was calibrated by using highly oriented pyrolytic graphite.

Results

Galvanostatic Reduction. As shown in Figure 1, two reduction potentials in galvanostatic cathodic reduction experiments at −2 μA cm^{-2} were observed at about −0.55 and −0.82 V/SCE for the passive films exposed to air for different duration. It is evident that a distinct first potential arrest gradually develops during air exposure, indicating the passive films tend to be gradually a "well-defined" state.

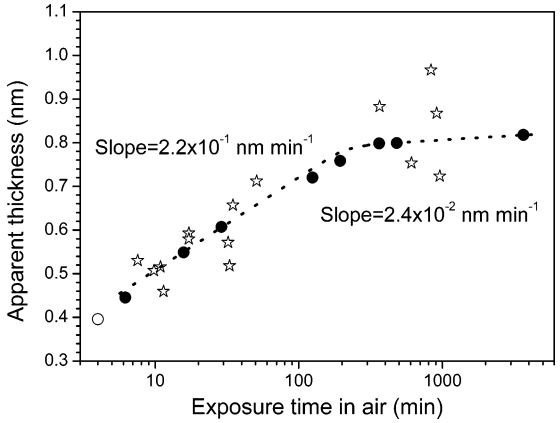

Figure 2. Evolution of the apparent film thickness with exposure time in air after passivation at −0.4 V/SCE for 30 min in borate buffer solution. The dotted line is the fitted line of all data. The data points marked by solid circles and an open circle are taken from the potential decay curves in Figure 1, and those marked by stars are from other separate experiments. The point marked by the open circle is a reference for film under exposure to nitrogen for a few minutes and no exposure to air after passivation.

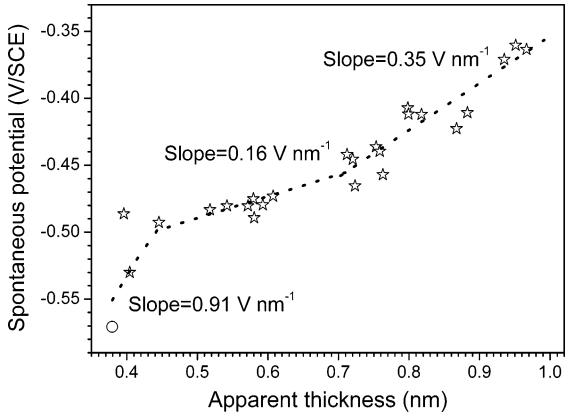

Figure 3. Dependence of spontaneous potential on the apparent thickness of passive films exposed to air after passivation at −0.4 V/SCE for 30 min in borate buffer solution. The dotted line is the fitted line of all data. The data point marked by an open circle is for film under exposure to nitrogen for a few minutes and no exposure to air after passivation.

Observations of two reduction potentials were frequently reported in cathodic reduction experiments that had been used to investigate the nature and stability of the Fe passive films.[1,3,13,31−36] The two-stage electrochemical dissolution mechanism in galvanostatic reduction was recently clarified by in situ XANES study.[34] The first potential plateau can be ascribed to the reductive dissolution as Fe^{2+} of Fe_3O_4 for galvanostatic reduction of both Fe_2O_3 and Fe_3O_4. After the complete reductive dissolution of Fe_3O_4, the potential abruptly drops to the second plateau (end potential), which corresponds to the equilibrium potential of bare Fe with the minor amount of a surface-trapped Fe^{2+} as a lower valent oxide in borate buffer solutions containing soluble Fe^{2+} ion. In situ XANES result indicated that the passive film at −0.8 V/MSE (−0.38 V/SCE) contains primarily Fe^{3+} ions with (17 ± 3)% Fe^{2+} ions,[36] which is similar to the mixture of 50% γ-Fe_2O_3 and 50% Fe_3O_4. Ex situ STM gave the observation that atomic arrays with hexagonal structure in the outermost surface are close to the oxygen array on the (111) oxygen planes of γ-Fe_2O_3.[23] Here, films formed at −0.4 V/SCE for 30 min are suggested to be a double-layer structure without well-defined interface and with the possible presence of Fe^{3+} and Fe^{2+} hydroxides on the surface (discuss below).

In light of the above assignations, the total reduction charge (C_t) of Fe^{3+} species as soluble Fe^{2+} is believed to be that at the intersection point between the tangent with the biggest potential decrease rate and the extended line of the end potential and its determination is shown in Figure 1. With the experimental error, reductive dissolution as soluble Fe^{2+} of γ-Fe_2O_3 and Fe_3O_4 and other Fe^{3+} species with a 100% current efficiency takes place during galvanostatic reduction in borate buffer solution.[34] From the total reduction charge as indicated in Figure 1, the apparent thickness of passive films can be evaluated as γ-Fe_2O_3 in terms of molecular weight (159.69 g mol^{-1}) and density (4.90 g cm^{-3})[33] and this indirectly reflects the content of all Fe^{3+} species in the passive film. Figure 2 gives the dependence of the apparent film thickness on the logarithm of the exposure time in air. Compared with the apparent film thickness under exposure to N_2 gas, there is a large increase from 0.40 to 0.80 nm after air exposure for 360 min. It is notable that the apparent film thickness (L_{app}) is rapidly increased with linear dependence on log t (i.e. $L_{app} \propto k_{app} \log t$, where the rate constant k_{app} is 2.2 × 10^{-1} nm min^{-1}) during the initial stages until about 130 min and slowly increases with a rate constant of 2.4 × 10^{-2} nm min^{-1} after a transition between 130 and 360 min. It is believed that the passive films formed at −0.4 V for 30 min are unstable and undergo a thickening with time during the initial stages of air exposure and become stable after air exposure for 360 min (i.e. t_s, the exposure time in air required for becoming the stable surface structure). This result is in agreement with that investigated by ^{18}O SIMS for passive films formed at −0.25 V/SHE (−0.49 V/SCE) for 60 min in ^{18}O-enriched borate buffer solution.[1] In the three experiments of air exposure for a few minutes and a long time (5 and 68 h), ^{18}O concentration in the former film is 4.9%, higher by 10% than the 4.4% in the latter two films, and the thickness is thinner by 20%. There is not so much difference in the ^{18}O concentration and thickness for the latter two films. ^{18}O concentrations in all three films are lower than 9.2% in the stable standard films,[1] indicating a thickening with exposure time in air.

A transition starting at 130 min as in Figure 2 is clearly demonstrated by the thickness dependence of the spontaneous potential of passive films exposed to air as shown in Figure 3. A spontaneous potential (E_S) is used to quantitatively describe the surface structure or the surface state of passive films and is defined here as the equilibrium chemical potential of the surface oxides when measured in borate buffer solution. E_S is believed to be approximately E_{OC} recorded within 10 s before galvanostatic reduction or E_{OC} decay measurements. Before exposure time t < 6 min in air, the spontaneous potential was increased by the highest rate as k_{sp} = 0.91 V nm^{-1}, thereafter by the lowest as 0.16 V nm^{-1} in the second region, and by the intermediate as 0.35 V nm^{-1} in the third region. It is implied that three different slopes possibly correspond to three different kinds of surface structures in three distinct linear dependent regions. Changes of surface structures that occurred in the three regions are possibly attributed to (1) the rapid dehydration of Fe^{3+} and Fe^{2+} hydroxides and partial rapid oxidation of Fe^{2+} species in the surface, (2) steady oxidation of Fe^{2+} species on the surface and in the underlayer, and (3) reconstruction of surface structures, respectively. It was previously reported[37] that the spontaneous potential depends on the existing Fe^{2+} ion concentration ([Fe^{2+}]) and pH in the addition of high [Fe^{2+}] (∼10^{-4} M). The addition of high [Fe^{2+}] masks the effect of the passivated potential and time (i.e. structures) on the spontaneous potential of passive films. In this work, there was a minor amount of Fe^{2+} ions (10^{-8} M) that resulted from the cathodic

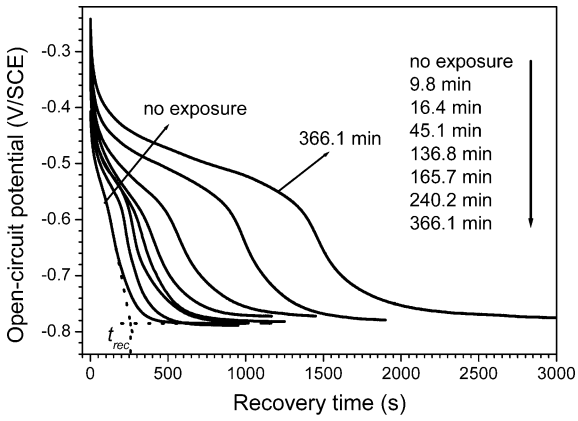

Figure 4. Open-circuit potential decay curves for passive films exposed to air for different durations after passivation at −0.4 V/SCE for 30 min in borate buffer solution. The dotted line indicates the determination of the recovery duration with <5% deviation. The arrow indicates the evolution of the open-circuit potential decay with exposure time in air.

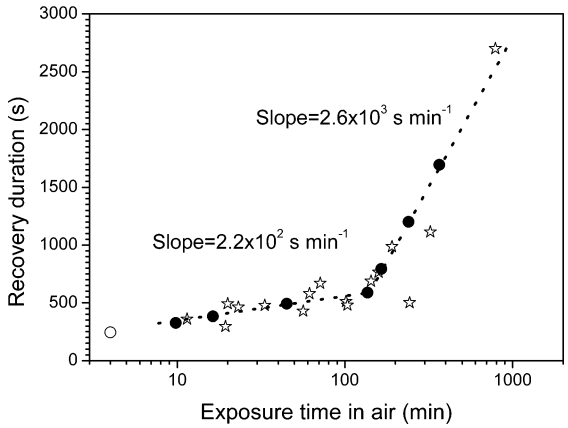

Figure 5. Dependence of recovery duration on exposure time in air for passive films formed at −0.4 V/SCE for 30 min in borate buffer solution. The dotted line is the fitted line of all data. The data points marked by solid circles and an open circle are taken from the open-circuit potential decay curves in Figure 4, and those marked by stars are from other separate experiments. The data point marked by an open circle is for film without air exposure after passivation.

reduction pretreatment of air-formed oxide films on the specimen's surface and metal dissolution in the initial stages of passive film growth. In addition, it is striking that two intersection points among three distinct linear dependent regions were observed at 0.45 and 0.71 nm, which correspond to the apparent thickness for passive films exposed to air for about 6 and 130 min, respectively. It is reasonably suggested that the exposure time of about 130 min in air is critical to the transformation of the surface structures of passive films formed at −0.4 V for 30 min.

Open-Circuit Breakdown. Figure 4 shows the effect of air exposure on the resistance of passive films formed at −0.4 V/SCE for 30 min against open-circuit breakdown in the borate buffer solution. In open-circuit potential decay to free corrosion potential of Fe (about −0.78 V), which is slightly affected by the Fe^{2+} concentration in the solution, a distinct first potential arrest was observed to develop with exposure time in air, indicating the passive films become more protective.

The previous investigations on the open-circuit breakdown of passive films,[31,32,37,38] or sputter-deposited oxide films,[39] or the air-formed oxide films[40,41] on Fe were done in borate buffer solutions. Although the details of the reaction mechanism during the course of the open-circuit experiments are still not completely clear, a mechanism of reductive dissolution rather than chemical dissolution was accepted to account for the production of Fe^{2+} not Fe^{3+} species in solution. Here, the slow decay of potential from the anodic region toward about −0.78 V is proposed to involve similar processes, i.e. the reductive dissolution of all Fe^{3+} species as soluble Fe^{2+}, as happened in galvanostatic reduction. Then the recovery duration (t_{rec}) is defined as the time required for the decay of the open-circuit potential from the anodic potential to the free corrosion potential of Fe or for the recovery of the electrode surface from the passive film to natural Fe, and its determination is indicated in Figure 4. The dependence of the recovery duration on exposure time in air is shown in Figure 5. A critical exposure time (t_c) at about 140 min was also noticeably observed, which is suggested to be in agreement with that observed in Figures 2 and 3 within the experimental error. After t_c, the recovery duration is drastically increased with linear dependence on log t (i.e. $t_{rec} \propto k_{rec} \log t$ where the rate constant $k_{rec} = 2.6 \times 10^3$ s min^{-1}) while there is a slow increase with a rate constant of 2.2×10^2 s min^{-1} during the initial stages of air exposure. It is indicated that another new passive state started at $t = t_c$ and the more protective structure was formed at $t > t_c$, which is consistent with the observations in galvanostatic reduction in the previous section.

The effect of air exposure on the apparent thickness and recovery duration of passive films formed at −0.4 V for 30 min is incorporated as follow. The apparent film thickness is rapidly increased by 78% from 0.40 nm at $t = 0$ to 0.71 nm at $t = t_c$ as seen in Figure 2, and the recovery time is rapidly increased by 140% from 245 s at $t = 0$ to 588 s at $t = t_c$ as seen in Figure 5. Whereas after exposure time $> t_c$, recovery duration drastically increases from 588 to 1690 s at $t = t_s$ and to 2700 s at $t = 800$ min as seen in Figure 5 and the apparent thickness slowly increases from 0.71 nm at $t = t_c$ to 0.80 nm at $t = t_s$ and becomes constant after $t > t_s$ as seen in Figure 2. It is found that a critical thickness of 0.71 nm at $t = t_c$ is required before passivity with more protection is established. Similar results were observed in conferring the stability of air-formed oxide film[41] and passive film[31,32,42] against open-circuit breakdown in borate buffer solutions. The critical thickness presented here is much less than those reported for air-formed oxide film (1.7 nm)[41] and passive film (1.3 nm).[42] Therefore it is inferred that crystal structures, especially surface crystal structures, play an important role in the resistance of passive films against open-circuit breakdown after a necessary oxide thickness is reached.

Nanoscale Observation. During the initial stages of air exposure, the surface structures drastically changed. It was difficult to observe the surface crystal structure before the surface structures became the "well-formed" state as indicated in Figure 2. After that, the surface crystal structures appeared as shown in Figure 6. It is evident that the nanocrystal structures with limited atoms, such as a cluster containing 19 atoms labeled A and a 2-nm atomic array with 1D short-range order labeled B, were observed after air exposure for 354 min as shown in Figure 6a. With increasing exposure time in air, the 10-nm atomic arrays with 1D long-range order in a 2-nm terrace, such as the atomic arrays labeled C and D, were observed at $t =$ 1710 and 1932 min in Figures 6b and 6c, respectively. At $t =$ 3111 min, the atomic array with quasi 2D long-range order was observed in Figure 6d though the terrace was still narrow in the step-terrace structure. With continued expose to air for 10181 min, the 5-nm-wide terrace with 2D long-rang order was clearly observed on the crystalline surface in Figure 7a, showing it to

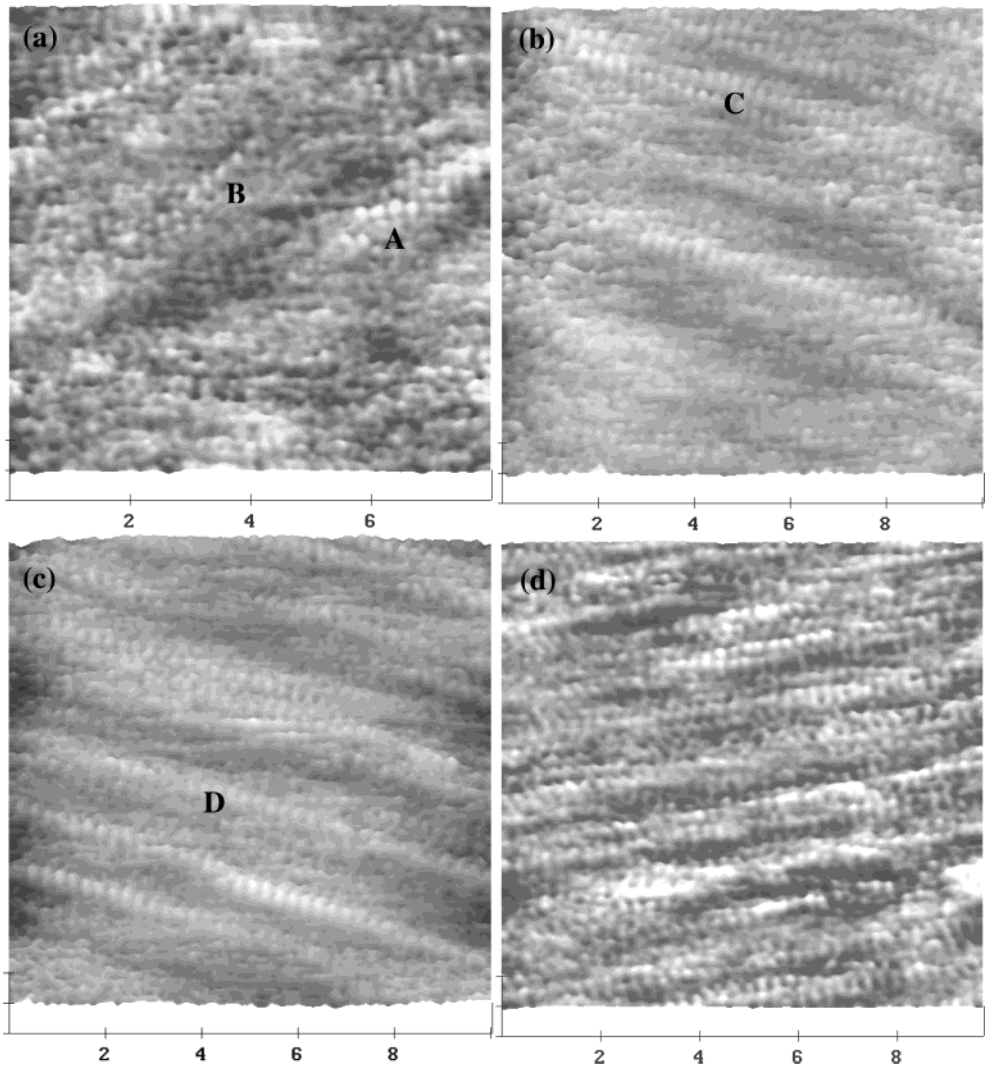

Figure 6. Atomically resolved STM images of passive films formed at −0.4 V/SCE for 30 min after air exposure for (a) 354, (b) 1710, (c) 1932, and (d) 3111 min. *XY* 2.0 nm/div, *Z* 0.5 nm/div. The distance between atoms or lattice constant in the ordered structure is (a) 0.29 ± 0.03, (b) 0.291 ± 0.004, (c) 0.298 ± 0.007, and (d) 0.281 ± 0.006 nm.

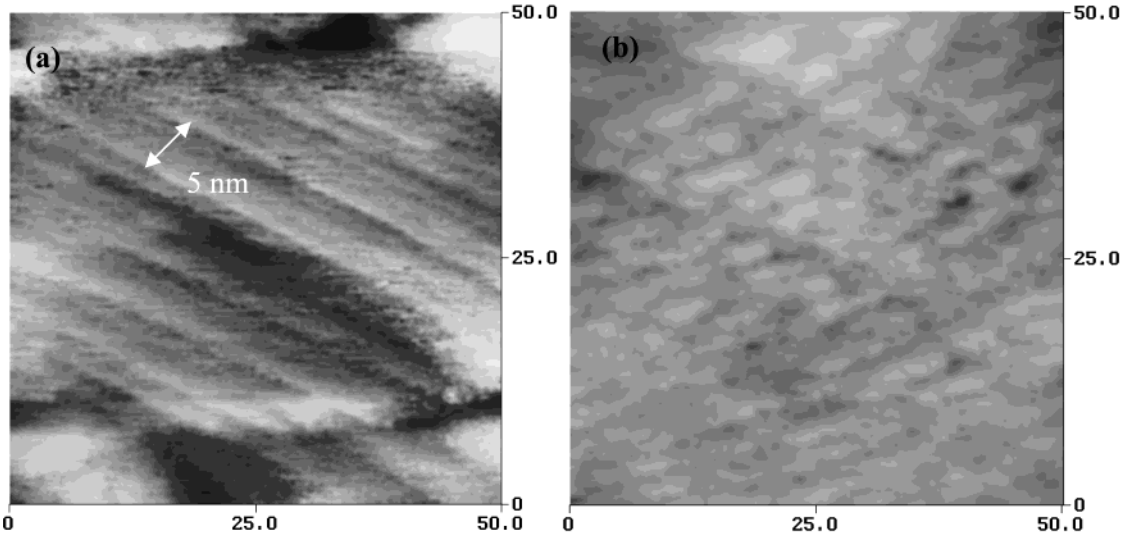

Figure 7. Surface morphology of passive films formed at −0.4 V/SCE for 30 min after air exposure for (a) 10181 min and (b) 1 month. *XY* 50 nm, *Z* 4 nm.

be more protective. Obviously, with exposure time in dry air, the terrace became wider expanding from 2 to 5 nm, and the crystallinity of surface structures was markedly improved from the amorphous structures to the crystalline so that the perfect defect-free crystalline structure would be achieved. If exposed to dry air for an excessive time, such as 1 month, the surface

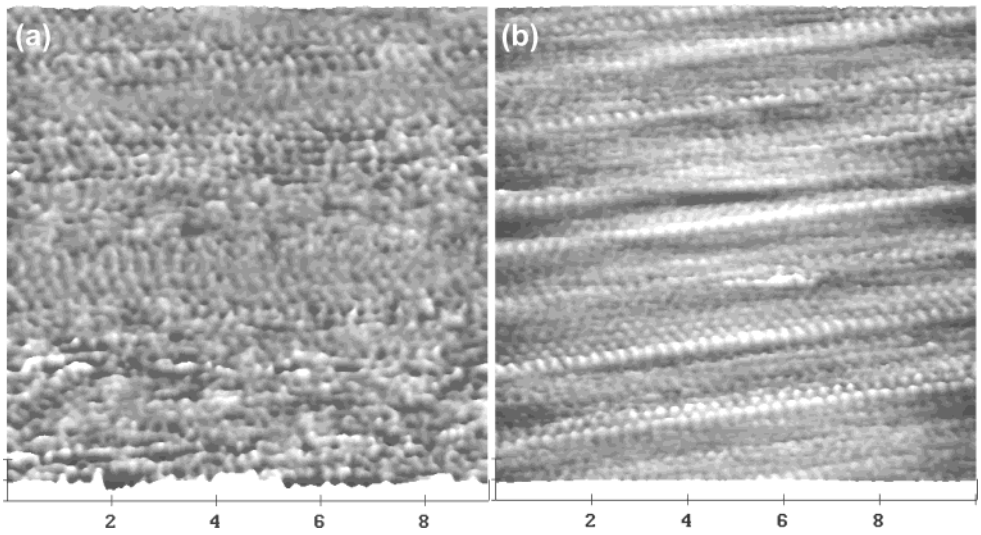

Figure 8. Atomically resolved STM images of passive films formed at −0.4 V/SCE for 30 min at 60 °C after air exposure for (a) 562 and (b) 3805 min. *XY* 2.0 nm/div, *Z* 0.3 nm/div. Lattice constant in the ordered structure is (a) 0.297 ± 0.008 and (b) 0.31 ± 0.03 nm.

structure in Figure 7a was partially deteriorated by natural degradation though the step-terrace structure can be distinguished in Figure 7b.

It is expected that passivation at −0.4 V at higher temperature would accelerate the recrystallization process in the borate buffer solution or shorten the recrystallization time in air.[23] In the following, STM observation of passive films formed at −0.4 V and 60 °C for 30 min demonstrated surface reconstruction in air at an atomic level. For passive films formed at −0.4 V and 60 °C for 30 min, it is also clearly demonstrated that the short-range ordered structure on the surface at $t = 562$ min in Figure 8a was converted to the 2D long-range ordered structure at $t =$ 3805 min in Figure 8b, around which the 5-nm terrace was also observed.[23] Compared with that for passivation at RT, the recrystallization time to become a long-range order structure in air was shortened from 10181 to 3805 min with passivation at higher temperature. This substantiates the assumption[23] that reconstruction in air within the identical exposure time does not shield the effect of passivation temperature on crystal structures of the surface when ex situ STM observation was applied to characterize the temperature effect.

The distances between atoms or lattice constants in the ordered structure as inserted in the captions of Figures 6 and 8 are close to the oxygen spacing on the (111) oxygen planes of γ-Fe_2O_3 (0.295 nm) and the inverse spinel structure of Fe_3O_4 (0.297 nm). It was observed in STM images that the lattice constant in the long-range order structure was 0.30 ± 0.01 nm for the passive film formed at 1.04 V/NHE (∼0.8 V/SCE).[18] Because the outer layer of the passive film contains mainly the composition of γ-Fe_2O_3,[12−17] the above ordered structures observed by STM are due to the γ-Fe_2O_3-like structure on an outermost surface. This assignation correlates well the in situ XANES result[36] that the passive film at −0.8 V/MSE (−0.38 V/SCE) contains primarily Fe^{3+} ions with 17% Fe^{2+} ions.

Discussion

During exposure to dry air (<30% RH), passive films formed at −0.4 V for 30 min undergo (1) rapid dehydration of Fe^{3+} and Fe^{2+} hydroxides and partial rapid oxidation upon removal from electrolyte solution and being rinsed with distilled water after passivation at $t < 6$ min, (2) steady air oxidation at $t < t_c$ until the attainment of a passive state to be more protective at $t = t_c$, and thereafter, (3) reconstruction from the amorphous state to short-range order and then to long-range order and further into perfect crystal structures with a wide terrace. These reconstruction processes gave rise to the significant change in the composition and surface structures of the passive films and remarkable improvement in the resistance of the passive films against open-circuit breakdown. It is worth pointing that the behavior of passive films formed at −0.4 V observed during air exposure is actually self-protective to further air oxidation.

With passivation at the low potential range between the onset of the passivity and −0.2 V/SCE, some Fe dissolution as Fe^{2+} ion prior to passivation had been observed in borate buffer solutions.[1,12,13,32,43] Ferrous ions in the solution arise from active dissolution of iron in the initial stages of the formation of passive films and the cathodic reduction of air-formed oxide in the pretreatment. These Fe^{2+} ions are precipitated as $Fe(OH)_2$ and converted into the porous layer of partially hydrated amorphous hydroxides of FeOOH or $Fe(OH)_3$,[8,37,44,45] which showed no contribution to the semiconducting properties.[44] It was detected by surface-enhanced Raman spectroscopy,[8−10,46] SIMS and X-ray photoelectron spectroscopy,[47] and Mössbauer spectroscopy[4−6] that the hydroxide-like species existed on the outer hydrated layer of passive films formed at the lower potential region of the Fe^{2+} appearance. As a result, the passive films revealed the low spontaneous potential as shown in Figure 3. Upon removal of passive films from the electrolyte solution after passivation at −0.4 V, rapid dehydration of hydroxides and rapid oxidation of Fe^{2+} species to Fe^{3+} species unavoidably take place in the initial stages of exposure to dry air. The dehydration of passive films gave rise to the distortion of the bond angle in the Fe−O/OH octahedral and resulted in the increase of Mössbauer quadrupole splitting.[4,5] The capture of the stable STM images supports the rapid conversion of Fe^{2+} species to Fe^{3+} species that happens at least on the outer layer of passive films. This is because the Fe^{2+} species acts as electron donor in n-type semiconducting Fe^{3+} passive films[48,49] and its energy levels are located within the forbidden band gap of the Fe^{3+} oxide semiconductor.[25,50] The Fe^{2+} species in passive films cannot be imaged at higher bias (1.2 V here) through the electron tunneling mechanism from the STM tip to the conduction band of passive films as investigated by electrochemical STM

TABLE 1: Reconstruction Processes Occurring during Air Exposure and Comparison of Rate Constants k_{sp}, k_{app}, and k_{rec} for Passive Films Formed at −0.4 V/SCE for 30 min

	exposure period			
	$t < 6$ min	6 min $< t < t_c$	$t_c < t < t_s$	$t > t_s$
k_{sp} (V nm^{-1})	0.91	0.16	0.35	
passive state	passivity I	passivity II	passivity III	
reconstruction in air	amorphous: dehydration of hydroxides and partial oxidation	amorphous: steady oxidation	1D order: oxidation in transition region	2D order: very slow oxidation
k_{app} (nm min^{-1})	$(2.2 \pm 0.3) \times 10^{-1}$	$(2.2 \pm 0.3) \times 10^{-1}$	transition region	$(2.4 \pm 0.3) \times 10^{-2}$
k_{rec} (s min^{-1})	−	$(2.2 \pm 0.7) \times 10^{2}$	$(2.6 \pm 0.3) \times 10^{3}$	$(2.6 \pm 0.3) \times 10^{3}$
k_{rec}/k_{app} (s nm^{-1})	−	10^3	−	1.1×10^5

measurements[25,50,51] and electrochemical impendence spectroscopic measurement.[51]

On the other hand, anodic current efficiency for the formation of passive films was low because a significant amount of Fe^{2+} was found in solution during the passivation at −0.4 V. Precipitation of ferrous ions and the conversion to the porous layer of amorphous oxides or/and hydroxides[8−10,44] in the initial stages of film growth delayed the attainment of passivity in borate buffer solutions. It was suggested that the passivation at −0.4 V and at RT for 675 s in borate buffer solution allows films to reach a primary passive state,[23] at which the passive film formed at −0.4 V protects the metal from further corrosion and through which Fe^{2+} ions cannot be easily transported. However, for the passive film formed at −0.4 V, it takes a longer time than 30 min to obtain the well-formed state (i.e. a complete passive state) and the passivation within 30 min does not establish the complete passivity.[23] As a result, the passive films showed the lowest spontaneous potential in Figure 3 and the poorest resistance against open-circuit breakdown in Figures 4 and 5. Upon exposure to air, the resistance of the passive films against open-circuit breakdown as shown in Figure 5 was remarkably improved, accompanying continuous oxidation and the rapid increase of the apparent thickness as shown in Figure 2. Three linear dependences of spontaneous potential with increasing the apparent thickness were shown in Figure 3 and their different k_{sp} values in the three-exposure period are listed in Table 1. On the basis of this result, the passive state of passive films is proposed to undergo three changes with the evolution of spontaneous potential schematically reflected in Table 1. At $t < 6$ min, the passive films in air have the same structure as that formed in borate buffer solution and are believed to be in the same passive state (passivity *I*) as the primary passivity attained in borate buffer solution though the spontaneous potential drastically increased as shown in Figure 3. At 6 min $< t < t_c$, a new passive state (passivity II) is believed to be attained and is different from passivity I as indicated by the different k_{sp} value. After $t > t_c$, the resistance against open-circuit breakdown was drastically enhanced in Figure 5 and the very slow increase in the apparent thickness occurred in Figure 2. It is inferred that the passive films with 0.71 nm thickness have almost completely covered the Fe surface at $t = t_c$ and another new passivity (passivity III) will start at $t = t_c$. In the following air exposure ($t_c < t < t_s$), the sequent increase of the apparent thickness indicates the complete passivity was not achieved on the surface yet. Fe^{2+} or iron species were continuously oxidized at those active sites where the surface had a higher number of defects or the underlying surface was exposed due to the diffusion of reactant species during the reconstruction. The recrystallization from short-range order to long-range order as described in the section of Nanoscale Observation further enhanced the resistance of passive films against open-circuit breakdown in Figures 4 and 5 even if the apparent thickness was constant after $t > t_s$. The formation of surface ordered γ-Fe_2O_3 structure on the surface of passive films well explained the reversible and irreversible changes of the Mössbauer spectra,[4,5] where these changes were reversible when films were dried for less than 5 h and irreversible after dehydration for 5 h. To take these results into account, the difference between passivity I and passivity II is believed to be attributed to the difference in the composition of the amorphous surface, and the difference between passivity II and passivity III is due to the large difference in the extent of the crystallinity on the crystalline surface.

The mechanism of passive film growth during air exposure was proposed to be oxygen inward transport as elucidated by ^{18}O SIMS investigation.[1] In that case the ^{18}O content curve starts at 2.5% at the outer surface and gradually decreases to 0.6% through the entire passive film at first formed at 0.35 V/SHE (0.11 V/SCE) for 1 h in solution without ^{18}O and additionally at 0.7 V/SHE (0.46 V/SCE) in 10% ^{18}O-enriched solution. If film growth was predominated by cation outward transport to the outer surface, the ^{18}O content at the outer surface would be 8% and would decrease rapidly to 0.02% at the oxide/metal interface.[52] Because ^{18}O was found at all depths within the entire oxide,[1] it was suggested that the transport process is more complex than a simple lattice diffusion of oxygen anions and the diffusion of oxygen anions via short-circuit paths is possibly involved in the transport process. From the 10-fold difference in k_{app} at $t < t_c$ and $t > t_s$ as listed in Table 1, it is inferred that at $t < t_c$, the transport process is dominated by short-circuit diffusion along high-diffusivity paths which are changeable during the growth process of passive films in air. With the growth of passive films in air, the short-circuit paths were gradually decreased and were eventually blocked as demonstrated by the change of rate constant k_{app} in a transition region in Figure 2. At $t > t_s$, the transport process is dominated by the lattice diffusion since the passive films were gradually recrystallized into long-range order as shown in Figures 7 and 8. This is also supported by the 10-fold difference in k_{rec} at $t < t_c$ and $t > t_c$ as listed in Table 1.

Electrons for reductive dissolution during open-circuit breakdown were supplied by anodic oxidation of metallic Fe. Anodic oxidation of Fe was controlled by the diffusion of cation vacancies at the film/solution interface to the metal/film interface through the entire oxide film,[31] rather than by the diffusion of Fe^{2+} ions at the film/solution interface into the bulk solution where the Fe^{2+} concentration is considered to be smaller. The diffusion coefficient of Fe^{2+} ions in $\sim 10^{-4}$ M solution was estimated as 5×10^{-6} cm^2 s^{-1} [37] by using the simple diffusion equation and in $\sim 10^{-8}$ M (the concentration of Fe^{2+} ions in this work) as 5×10^{-10} cm^2 s^{-1}. The diffusion coefficient of the cation in the passive film on iron is 2×10^{-16} cm^2 s^{-1} [53] obtained by a best fit to experimental data and is 2 orders of magnitude larger than the lattice diffusion coefficient (D_{bulk}) of

10^{-18} cm^2 s^{-1} [54] approximated by atomistic modeling and transition state theory. In the effective diffusion-coefficient model,[55] a diffusion coefficient of the cation in the passive film on iron is the sum of the bulk and grain boundary coefficients (D_{gb}), i.e. $D_{eff} = \phi D_{gb} + (1 - \phi)D_{bulk}$, where ϕ is the fraction of the cross-sectional area occupied by grain boundary. For $\phi = 5\%$, D_{eff} is taken as 2×10^{-16} cm^2 s^{-1} and D_{gb} is evaluated as 4×10^{-15} cm^2 s^{-1}, 3 orders of magnitude larger than D_{bulk} when grain boundary diffusion dominates cation transport. The ratios of $k_{app}(t<t_c)/k_{app}(t>t_s)$ and/or $k_{rec}(t>t_c)/k_{rec}(t<t_c)$ as indicated in Table 1 are very close to the square root of D_{eff}/D_{bulk}, which implies that the transport of cation vacancies along short-circuit paths such as grain boundaries or dislocations is dominant at $t < t_c$. With recrystallization in air of passive films (especially for surface structures), the short-circuit paths for the transport of cation vacancies during open-circuit breakdown were gradually decreased until they were eventually blocked and the lattice diffusion is dominant at $t > t_c$. Therefore the 10-fold difference in k_{rec} at $t < t_c$ and $t > t_c$ as indicated in Table 1 can be utilized to differentiate the diffusion mechanism of cation vacancies between $t < t_c$ and $t > t_c$ during open-circuit breakdown. Cation vacancies transport along short-circuit paths at $t < t_c$ and through the lattice diffusion in the passive film at $t > t_c$.

In addition, it is emphasized that crystal structures (*or* surface crystal structures) have large contributions to the resistance against open-circuit breakdown in borate buffer solution, whereas the crystal structures play no remarkable role in the galvanostatic reduction controlled only by the diffusion of Fe^{2+} ions at the film/solution interface into the bulk solution. This is demonstrated by the fact that there is a large difference in the ratio of k_{rec} to k_{app} between $t < t_c$ and $t > t_c$ as listed in Table 1. At $t < t_c$, the recovery duration is proportional to the apparent thickness of passive films because reductive dissolution in open-circuit breakdown is limited by the diffusion along the short-circuit paths. The recovery time mainly depends on the crystal structures rather than the apparent thickness at $t > t_c$ when reductive dissolution in open-circuit breakdown is limited by the lattice diffusion. This is also supported by another set of separate experiments described as follows. After passive film was exposed to air for 72 h, its open-circuit potential decay was observed from −0.34 to −0.43 V during immersion in borate buffer solution for 330 min. The remainder of the passive film showed an apparent thickness of 0.76 nm, characterized by the following galvanostatic cathodic reduction at -2 μA cm^{-2}. That is to say, only a 0.06-nm-thick layer was reductively dissolved within the 330-min measurement of open-circuit breakdown because an average apparent thickness was 0.82 nm for the passive film formed at −0.4 V for 30 min and exposed to air for 72 h. These results mean that the open-circuit potential decay curve is more sensitive to the crystal structures of passive films after a necessary thickness for the passivity was attained at $t = t_c$. From the discussions mentioned above, open-circuit measurement in combination with galvanostatic reduction is possibly used to quantitatively describe the extent of the crystallinity of passive films.

Conclusions

(1) During exposure in dry air (<30% RH), the apparent film thickness of passive films formed at −0.4 V is rapidly increased with linear dependence on log t where the rate constant of film growth is 2.2×10^{-1} nm min^{-1} in the initial stages until about 130 min. After a transition between 130 and 360 min, it slowly increases with the rate constant of 2.4×10^{-2} nm min^{-1} in the following stages, and the changes of surface structures from the amorphous state to short-range order and then to long-range order and further to crystal structures with a wide terrace were observed. These processes are suggested to be attributed to rapid dehydration of Fe^{3+} and Fe^{2+} hydroxides and partial rapid oxidation upon removal from electrolyte solution after passivation, steady air oxidation until the attainment of a passive state to be more protective one at $t = t_c$, and reconstruction in air, respectively.

(2) The reconstruction process in air drastically improved the resistance of the passive films against open-circuit breakdown after a critical exposure time was reached. After t_c, the recovery duration is rapidly increased with linear dependence on log t with a rate constant of 2.6×10^3 s min^{-1}, while there is a slow increase with a rate constant of 2.2×10^2 s min^{-1} during the initial stages of air exposure. It is indicated that another new passive state started at $t = t_c$ and the more protective structure was formed at $t > t_c$. The behavior of passive films formed at −0.4 V observed during air exposure is actually self-protective.

(3) The growth mechanism of passive films during air exposure was discussed. It is suggested that the process of oxygen inward transport is dominated by the diffusion along short-circuit paths at $t < t_c$. With the growth of passive films in air, the short-circuit paths were gradually decreased at $t > t_c$ and were eventually blocked. At $t > t_s$, the transport process is dominated by the lattice diffusion since the passive films was gradually crystallized into long-range order. The similar mechanism seems to play an important role in the open-circuit breakdown where cation vacancies are diffused from the film/solution interface to the metal/film interface through the entire oxide film.

Acknowledgment. H. H. Deng, the fellow of the Cooperative System for Supporting Priority Research by the Japan Science and Technology Corporation, is grateful for the support from the system. The authors thank Dr. T. M. Suzuki (Laboratory for Membrane Chemistry, AIST Tohoku, AIST, Japan) and Dr. P. Qian (Honda R&D Co. Ltd, 1-4-1, Chuo, Wako 351-0193, Japan) for their helpful discussions.

References and Notes

(1) Goetz, R.; Mitchell, D. F.; MacDougall, B.; Graham, M. J. *J. Electrochem. Soc.* **1987**, *134*, 535.
(2) Graham, M. J.; Bardwell, J. A.; Goetz, R.; Mitchell, D. F.; MacDougall, B. *Corros. Sci.* **1990**, *31*, 139.
(3) Bardwell, J. A.; Sproule, G. I.; Mitchell, D. F.; MacDougall, B.; Graham, M. J. *J. Chem. Soc., Faraday Trans.* **1991**, *87*, 1011.
(4) Eldridge, J.; Hoffman, R. W. *J. Electrochem. Soc.* **1989**, *136*, 955.
(5) O'Grady, W. E. *J. Electrochem. Soc.* **1980**, *127*, 555.
(6) Eldridge, J.; Kordesch, M. E.; Hoffman, R. W. *J. Vac. Sci. Technol.* **1982**, *20*, 934.
(7) Rubim, J. C.; Dunnwald, J. *J. Electroanal. Chem.* **1989**, *258*, 327.
(8) Rubim, J. C. *J. Electrochem. Soc.* **1993**, *140*, 1601.
(9) Cui, J.; Devine, T. M. *J. Electrochem. Soc.* **1991**, *138*, 1376.
(10) Schroeder, V.; Devine, T. M. *J. Electrochem. Soc.* **1999**, *146*, 4061.
(11) Davenport, A. J.; Sansone, M. *J. Electrochem. Soc.* **1995**, *142*, 725.
(12) Oblonsky, L. J.; Davenport, A. J.; Ryan, M. P.; Isaacs, H. S.; Newman, R. C. *J. Electrochem. Soc.* **1997**, *144*, 2398.
(13) Nagayama, M.; Cohen, M. *J. Electrochem. Soc.* **1962**, *109*, 781.
(14) Foley, C. L.; Kruger, J.; Bechtoldt, C. J. *J. Electrochem. Soc.* **1967**, *114*, 994.
(15) Kuroda, K.; Cahan, B. D.; Nazri, G.; Yeager, E.; Mitchell, T. E. *J. Electrochem. Soc.* **1982**, *129*, 2163.
(16) Toney, M. F.; Davenport, A. J.; Oblonsky, L. J.; Ryan, M. P.; Vitus, C. M. *Phys. Rev. Lett.* **1997**, *79*, 4282.
(17) Davenport, A. J.; Oblonsky, L. J.; Ryan, M. P.; Toney, M. F. *J. Electrochem. Soc.* **2000**, *147*, 2162.
(18) Ryan, M. P.; Newman, R. C.; Thompson, G. E. *J. Electrochem. Soc.* **1995**, *142*, L177.
(19) Rees, E. E.; Ryan, M. P.; McPhail, D. S. *Electrochem., Solid State Lett.* **2002**, *5*, B21.

(20) Bhardwaj, R. C.; Gonzalez-Martin, A.; Bockris, J. O'M. *J. Electrochem. Soc*. **1991**, *138*, 1901.
(21) Li, J.; Meier, D. J. *J. Electroanal Chem.* **1998**, *454*, 53.
(22) Díez-Pèrez, I.; Gorostiza, P.; Sanz, F.; Müller, C. *J. Electrochem. Soc*. **2001**, *148*, B307.
(23) Deng, H. H.; Qian, P.; Sanada, N.; Yoneya, M.; Nanjo, H. *J. Electrochem. Soc.* **2003**, *150*, B336.
(24) Sewell, P. B.; Stockbridge, C. D.; Cohen, M. *J. Electrochem. Soc*. **1961**, *108*, 933.
(25) Brett, M. E.; Parkin, K. M.; Graham, M. J. *J. Electrochem. Soc*. **1986**, *133*, 2031.
(26) Oblonsky, L. J.; Devine, T. M. *Corros. Sci*. **1995**, *37*, 17.
(27) Ryan, M. P.; Newman, R. C.; Thompson, G. E. *Philos. Mag*. **1994**, *70*, 241.
(28) Nanjo, H.; Newman, R. C.; Sanada, N. *Appl. Surf. Sci*. **1997**, *121*/*122*, 253.
(29) Ryan, M. P.; Newman, R. C.; Thompson, G. E. *J. Electrochem. Soc*. **1994**, *141*, L165.
(30) Maurice, V.; Yang, W. P.; Marcus, P. *J. Electrochem. Soc*. **1996**, *143*, 1182.
(31) Bardwell, J. A.; MacDougal, B.; Graham, M. J. *J. Electrochem. Soc*. **1988**, *135*, 413.
(32) Bardwell, J. A.; Graham, M. J. *J. Electrochem. Soc*. **1988**, *135*, 2157.
(33) Büchler, M.; Schmuki, P.; Böhni, H. *J. Electrochem. Soc*. **1997**, *144*, 2307.
(34) Schmuki, P.; Virtanen, S.; Davenport, A. J.; Vitus, C. M. *J. Electrochem. Soc*. **1996**, *143*, 574.
(35) Ogura, K.; Majima, T. *Electrochim. Acta* **1978**, *25*, 1361.
(36) Oblonsky, L. J.; Davenport, A. J.; Ryan, M. P.; Isaacs, H. S.; Newman, R. C. *J. Electrochem. Soc*. **1997**, *144*, 2398.
(37) Nagayama, M.; Cohen, M. *J. Electrochem. Soc*. **1963**, *110*, 670.
(38) Cahan, B. D.; Chen, C. T. *J. Electrochem. Soc*. **1982**, *129*, 921.
(39) Pryor, M. J.; Evans, U. R. *J. Chem. Soc., Chem. Commun.* **1950**, 1259.
(40) Gilroy, D.; Mayne, J. E. O. *Br. Corros. J.* **1965**, *1*, 102.
(41) Konno, H.; Kawai, M.; Nagayama, M. *Surf. Technol*. **1985**, *24*, 259.
(42) Pinkowski, A. *Werkst. Korros*. **1982**, *37*, 526.
(43) Moshtev, R. V. *Ber. Bunsen-Ges. Phys. Chem*. **1968**, *72*, 452.
(44) Büchler, M.; Schmuki, P.; Böhni, H. *J. Electrochem. Soc*. **1998**, *145*, 609.
(45) Ohtsuka, T.; Ju, J. C.; Ito, S.; Einaga, H. *Corros. Sci*. **1994**, *36*, 1257.
(46) Oblonsky, L. J.; Virtanen, S.; Schroeder, V.; Devine, T. M. *J. Electrochem. Soc*. **1997**, *144*, 1604.
(47) Tjong, S. C.; Yeager, E. *J. Electrochem. Soc*. **1981**, *128*, 2251.
(48) Schmuki, P.; Büchler, M.; Virtanen, S.; Böhni, H.; Müller, R.; Gauckler, L. J. *J. Electrochem. Soc*. **1995**, *142*, 3336.
(49) Büchler, M.; Schmuki, P.; Böhni, H.; Stenberg, T.; Mäntylä, T. *J. Electrochem. Soc*. **1998**, *145*, 378.
(50) Schreger, A.; Eng, L.; Böhni, H. *J. Vac. Sci. Technol.* **1996**, *B14*, 1162.
(51) Díez-Pèrez, I.; Gorostiza, P.; Sanz, F. *J. Electrochem. Soc*. **2003**, *150*, B348.
(52) Atkinson, A. *Rev. Mod. Phys.* **1985**, *57*, 437.
(53) Battaglia, V.; Newman, J. *J. Electrochem. Soc*. **1995**, *142*, 1423.
(54) Atkin, J.; Hendy, S.; Laycock, N.; Mackay, J.; Nanjo, H.; Ryan, M. P. *Atomistic Modeling of the Passive Film on Iron*; 204th meeting of the Electrochemical Society, Florida, 2003; Abstract 1301.
(55) Laycock, N.; Ryan, M. P.; Hendy, S.; Krouse, D.; Atkin, J.; Mackay, J.; Nanjo, H. *Modeling the Formation and Localized Breakdown of Passive Films*; Proceedings of AIST-ISEM International Symposium, AIST03-K00010, Nagoya, Japan, 2003; pp 51−62.